AD_____

Award Number: W81XWH-09-1-0734

TITLE: A Wireless Sensor System for Real-Time Measurement of Pressure Profiles at Lower Limb Protheses to Ensure Proper Fitting

PRINCIPAL INVESTIGATOR: Keat Ghee Ong, Ph.D.

CONTRACTING ORGANIZATION: Michigan Technological University
Houghton, MI 49931

REPORT DATE: October 2011

TYPE OF REPORT: Annual

PREPARED FOR: U.S. Army Medical Research and Materiel Command
Fort Detrick, Maryland 21702-5012

REPORT DOCUMENTATION PAGE

Form Approved
OMB No. 0704-0188

1. REPORT DATE	2. REPORT TYPE	3. DATES COVERED
October 2011	Annual	18 September 2010 – 17 September 2011

4. TITLE AND SUBTITLE

A Wireless Sensor System for Real-Time Measurement of Pressure Profiles at Lower Limb Protheses to Ensure Proper Fitting

5a. CONTRACT NUMBER

5b. GRANT NUMBER
W81XWH-09-1-0734

5c. PROGRAM ELEMENT NUMBER

6. AUTHOR(S)

Keat Ghee Ong
Brandon Pereles
Andrew DeRouin
E-Mail: kgong@mtu.edu

5d. PROJECT NUMBER

5e. TASK NUMBER

5f. WORK UNIT NUMBER

7. PERFORMING ORGANIZATION NAME(S) AND ADDRESS(ES)

Michigan Technological University
Houghton, MI 49931

8. PERFORMING ORGANIZATION REPORT NUMBER

9. SPONSORING / MONITORING AGENCY NAME(S) AND ADDRESS(ES)
U.S. Army Medical Research and Materiel Command
Fort Detrick, Maryland 21702-5012

10. SPONSOR/MONITOR'S ACRONYM(S)

11. SPONSOR/MONITOR'S REPORT NUMBER(S)

12. DISTRIBUTION / AVAILABILITY STATEMENT
Approved for Public Release; Distribution Unlimited

13. SUPPLEMENTARY NOTES

14. ABSTRACT

The goal of this project is to perform initial development of a new sensor system for ensuring proper fitting of a lower limbprosthesis by providing real-time monitoring of pressure distribution at the body-prosthesis interface. To date, we have completed the design, fabrication, and optimization of the base sensing platform, a three strip sensor. Specifically, we have constructed a sensing layer that can be placed on a hard surface for measuring force loading. To evaluate the efficacy of the sensor, we have also constructed an automated pneumatic mechanical loader and the interface controlling circuits for the loader, an algorithm has been developed. The next step is to develop a the base technology into a grid like mapping sensor, construct the excitation and detection circuits, modify and optimize the algorithm, and embed the sensor.

15. SUBJECT TERMS
Wireless, magnetoelastic, lower limb prosthesis.

16. SECURITY CLASSIFICATION OF:			17. LIMITATION OF ABSTRACT	18. NUMBER OF PAGES	19a. NAME OF RESPONSIBLE PERSON
a. REPORT	b. ABSTRACT	c. THIS PAGE			USAMRMC
U	U	U	UU	30	19b. TELEPHONE NUMBER *(include area code)*

Table of Contents

Introduction

The goal of this project is to perform initial development of a new sensor system for ensuring proper long term fitting of a lower limb prosthesis by providing real-time monitoring of pressure distribution at the body-prosthesis interface. To date, we have completed the design, fabrication and optimization of the base sensing platform, the sensor, and currently have a paper submitted for review and possible publication. Specifically, we have constructed a sensing layer capable of monitoring force on hard surfaces (see **Appendix A** for the submitted article). To evaluate the efficacy of the sensor, we constructed an automated pneumatic mechanical loader, implemented the interface controlling circuits for the loader and developed an algorithm for data analysis. Additionally, a detection circuit has also been designed and is being finalized. The current phase of the project involves advancing the base technology into a grid-like mapping sensor, constructing the excitation and detection circuits, modifying and optimizing the algorithm and embedding the sensor.

Body

The focus of this project is the development of a prototype sensor system capable of measuring pressure profiles at the socket-stump interface of a lower limb prosthesis. The specific aims of this project are (1) Fabrication of the Sensing Layer, (2) Development of the Detection System and (3) System Performance Evaluation.

Specific Aim 1: Fabrication of the Sensing Layer

Task 1A: Sensing Layer Fabrication

We previously reported on three investigated techniques for fabricating the sensing layer and at this phase of the project the use of Metglas is still ideal due to its high stress sensitivity; however, a highly desirable technique for fashioning sensors from Metglas, screen printing and etching, has been tested. Additionally, this technique has also allowed for preliminary testing of non-uniform shaped sensing strips capable of measuring four loading points. Furthermore, initial investigation into embedding the Metglas sensors has also been performed.

Screen Printing and Etching: Previously, a shearing method was utilized to fashion sensing strips. While the shearing technique produces sensors with good magnetic and magnetoelastic properties, it is difficult to control the reproducibility thus creating a challenge for making a uniform sensing layer. As a result, a new technique for fabricating these strips based on screen printing and etching has been developed.

The screen printing and etching technique first involves the fabrication of an enamel mask, with the desired designs, that is placed over a fine wire mesh screen. Once the screen and mask are prepared, the strips are adhered to a polycarbonate block using double sided adhesive film, and then placed on the chuck of the screen printing machine. Tests are then performed to ensure that the appropriate amount of pressure is applied by each of the squeegees, with the first squeegee being used for spreading applied paint and the second being used for pushing applied paint through the screen onto the strips. Following this, a mixture of 5900 Series Enamel Plus Gloss Screen Ink (Nazdar Shawnee Facility, 8501 Hedge Lane Terrace Shawnee, KS U.S.A.) and 9050 Retarder Thinner (Nazdar Shawnee Facility, 8501 Hedge Lane Terrace Shawnee, KS U.S.A.) is applied on the screen, around the designs and on the squeegees. The machine then takes over with an automated paint application process. The strips are then baked at 85 °C for one hour and allowed to cool. The strip now has the appropriate protective coatings and can be etched.

Prior to etching, a small beaker is filled with ferric chloride and placed onto a hotplate set to 45 °C. While the solution is heating up, the screen printed strips are sheared in order to produce smaller strips each containing one coated design. These smaller strips are then attached to a specially designed apparatus for holding the strips during the etching process using double sided adhesive tape. The apparatus consists of a polycarbonate block with a hole drilled through the bottom in order to accommodate a magnetic stir stick. This is necessary in order to not only provide constant motion of the strips in the etching solution, but to also expedite the process. Once the solution reaches 45 °C, the apparatus is submerged and the magnetic stirring is turned on. It is important to observe the etching process every 10 minutes, especially near the 20 minute mark, because, while it is necessary to ensure that all uncoated material is removed, if the strips are etched for too long the exposed sides of the coated areas can be over etched resulting in curving and other undesirable shape effects at the edges.

Non-Uniform Sensor Design: The use of screen printing and etching has also inspired the fabrication and preliminary testing of sensing strips with non-uniform geometry between the

front and back halves of the strip (see **Fig. 1**). In theory, when the length of the sensing strip moves away from a detection coil, the strength of the captured magnetic field from a particular portion of the strip decreases.

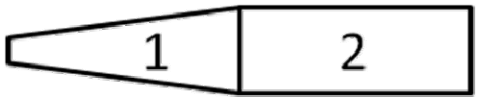

Fig. 1. Non-symmetric sensing strip design capable of acting as a 2×1 sensor, with regions 1 and 2 denoting different force sensing areas.

As a result, the back half of a strip will appear to have a weaker overall response than the front half. This means that the front and back halves of a strip can be thought of as two different sensing elements, theoretically allowing a single strip to measure forces at two pressure points.

In order for the sensing strip to function, there must be a distinguishable difference in sensor response when applying loads from the front/back halves of the strip (i.e. region 1 and region 2 respectively). While this effect has been demonstrated in rectangular strips, the result of loading only region 2 is not sensitive enough for this application; however, if the strip is rotated 180 degrees, then region 1 becomes region 2 and, by quantifying the effect of loading in these orientations, force can be monitored in both regions (in actual use there will be detection coils monitoring both ends of the strips). Unfortunately, the geometric symmetry of a rectangular strip presents a problem in that the response of the rotated strip is the same as the unrotated response. Additionally, even if the loading can be determined, which region the loading is from cannot be discovered without visual inspection of the test conditions, whereas in the ideal case only analysis software will be utilized to determine the force location.

To solve this problem, half rectangular-half trapezoid shaped sensing strips were proposed and preliminary testing of sheared sensing strips has been performed. **Fig. 2** illustrates the response of a rectangle and a trapezoidal strip when loaded in region 1 and 2, for both rotated and unrotated orientations, while **Fig. 3** illustrates a rectangular/trapezoidal sensing strip measured while loading regions 1 and/or 2 under both orientations.

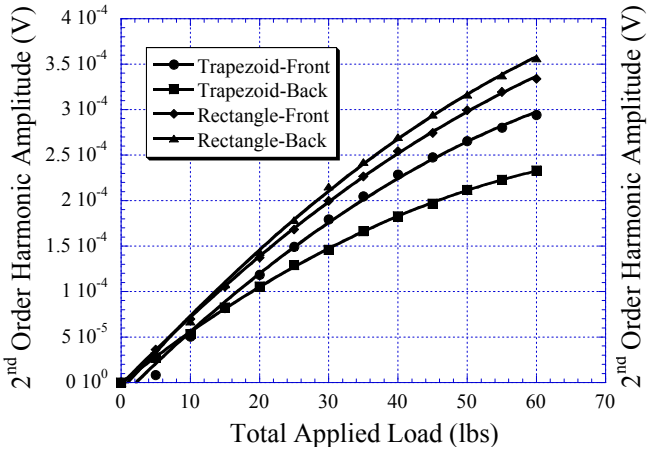

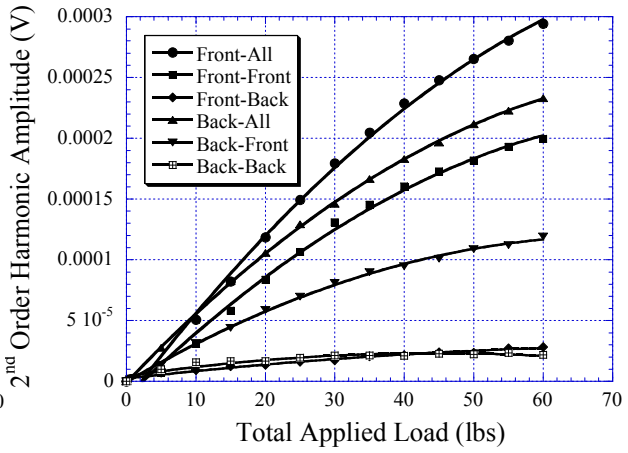

Fig. 2. (left) Preliminary testing demonstrating the difference in sensor response when loading regions 1 and 2 of a rectangular and trapezoidal sensing strip while measuring from the front (unrotated) and back (rotated) orientations.

Fig. 3. (right) Preliminary testing of a trapezoidal sensor while loading regions 1 and/or 2 from the relative front/back of the strip.

As can be seen, measurements from the rectangular strip have little difference in either orientation when loading in region 1 and/or 2. On the other hand, the trapezoidal sensor design illustrates a distinct difference not only between loading in regions 1 and 2, but also between both sensor orientations. It is theorized that this results not only from a difference in the amount of material under load, which contributes to the overall magnetic field strength, but also the effect that the non-symmetric geometry has on the magnetic field lines. This is currently only a theory and has yet to be investigated further.

In conclusion, the screen printing and etching process allows for precise repeatable production of sensing elements for grid fabrication. Moreover, the process allows for the exploration of the effects of non-uniform strip design on overall sensor performance. The next step in this process is to fully characterize a two strip trapezoidal sensor design for measuring four pressure positions.

Embedded Sensor: Preliminary investigations into embedding the sensors have also been performed. Sensing strips were embedded, in soft polyurethane rubber, inside of a well milled into a piece of polycarbonate. **Fig. 4** displays results from preliminary embedded sensor testing and, unlike data collected when the sensor was placed on a hard surface (see **Fig. 5a-c** of the submitted journal article in **Appendix A**), there is an initial downward trend in the data followed by an upswing.

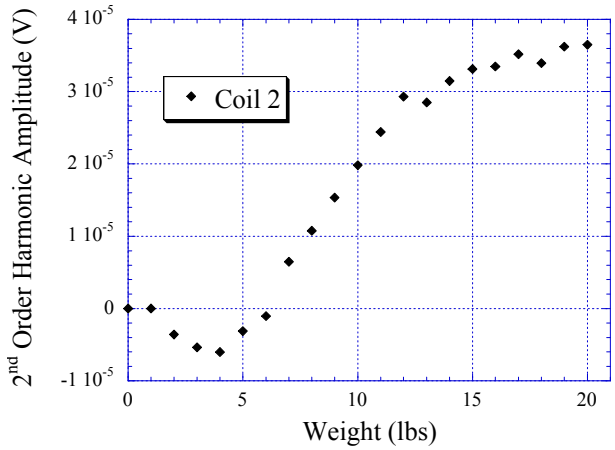

Fig. 4. The response of an embedded rectangular sensing strip under loading

Although this effect has not been thoroughly investigated yet, it is theorized that this may be a result of sensor movement during compression of the embedding material and/or the effects of tensile/compressive forces on the sensor during material compression. These results will be further explored following the development of the sensing grid.

Task 1B: Sensing Strip Optimization

The new fabrication technique with screen printing has significantly reduced the internal stress of the sensing strip. As a result, the as-fabricated strips have relatively good magnetic and magnetoelastic properties. Nevertheless, to ensure all residue stress in the strips was removed, all sensors were annealed in vacuum (-600psi) at 250 °C for 1 hr.

Specific Aim 2: Development of the Detection System

Task 2A: Detection/Excitation Circuit Fabrication

Excitation Circuit: To eliminate the need for external AC and DC power supplies, a driving circuit was designed. A Wein Bridge oscillator generated a sinusoid which was then fed through a fourth order multiple-feedback filter. Next, an amplifier with a class AB output stage employing TIP42 and TIP43 high-power transistors provided the power amplification necessary to obtain field strengths comparable to the original AC supply and audio amplifier combination.

For the DC supply circuitry, a DAC output from the microcontroller was amplified with a TIP33C transistor placed in the feedback loop of an op amp. Use of the DAC voltage was desired to enable a programmable DC biasing sweep of the sensors. The LF356 was selected for coupling with the TIP33C due to its similarity to the LF353 with increased capabilities when driving reactive loads.

Harmonic Detection Circuit: A more efficient method of detection was required to combat the problem of slow detection speeds incurred by sampling coils in series. To that end, a method of sampling in parallel was devised which involved multiple lock-in detection circuits measured concurrently by a microcontroller. Additionally, since only the second harmonic is desired, the detection frequency was set at 400 Hz to eliminate the need for an entire spectrum.

Lock-in amplification involves the multiplication of the input signal with a reference sinusoid followed by low-pass filtering. Multiplication of sine waves has the effect of generating two new sine waves: one at a frequency $f_1 - f_2$ and one at $f_1 + f_2$. When the reference and input sinusoid are of the same frequency, the result is a DC voltage plus a sinusoid at the square of the signals' frequencies. The result of multiplying all signals of dissimilar frequency will be an AC signal component. By low-pass filtering, the DC voltage can be isolated, correlating to the RMS voltage of the input component at the frequency of the reference. Because the multiplied signal results are dependent on the phase between the reference and input sinusoids, an additional step must be taken to repeat the multiplication and filtering process with a reference offset by 90 degrees from the original. It is then possible to extract the magnitude information by applying the Pythagorean Theorem to the unshifted and shifted results. Similarly, the phase can be determined by taking the inverse tangent of the signal in relation to the reference.

The input signal from the coil was first acquired with an AD8220 instrument amplifier input stage for high CMMR. The instrument amplifier was followed by a 60 Hz notch filter and a fourth-order band-pass filter with a gain of 100 at a center frequency of 400 Hz. The amplified and filtered signal was then multiplied with a reference signal generated by a Wein Bridge oscillator circuit at 400 Hz. The multiplier selected for this application was the AD835 4-quadrant multiplier due to its fast settling time, low noise, high input impedance and minimal requirement for external components. The input signal was also multiplied by a version of the reference frequency fed through a 90 degree phase-shifting circuit. After multiplication, second-order low-pass Butterworth filters extracted the DC signal from the two outputs. The current status of the circuit proves its ability to extract the DC level based on frequency and phase but has yet to be integrated with a microcontroller and the rest of the system.

Task 2B: Detection Coil Fabrication

New detection coils and a new faceplate were constructed. A custom built manual coil winder, with a rotary counter, provided a simple method for ensuring a consistent number of turns on each coil and, as a result, the same or nearly the same impedance. Additionally, previous errors in detection coil construction were minimized by using a VFlash 3D printer to construct the coil frames. Wound coils were attached to a new faceplate, fabricated using a CNC Micro Milling Machine, which was then screwed onto the excitation coil.

Task 2C: Algorithm Development

We previously reported the development of a linear multivariable analysis technique to determine the applied load as a function of 2nd order harmonic amplitude. However, the new automated loader has allowed for the collection of more precise data which has more clearly shown what the relationship between applied load and 2nd order harmonic amplitude appears to be.

Linear Multivariable Analysis: The previously presented algorithm relied on the use of linear multivariable analysis. In essence, analysis of data collected prior to the automated systems led to the conclusion that the relationship between applied load and 2nd order harmonic amplitude could be linearized and, thus, placed into a series of matrices which could be easily manipulated to find force. The previously used model was abandoned when it was discovered that the relationship between applied force and 2nd order harmonic amplitude more closely resembled a decaying exponential function which, while capable of being linearized, has multiple roots, thus making the linearization unreliable. Additionally, an exponential curve model fits with the theoretical description of the permeability change in response to force described in section 2.3 of the appended journal article in **Appendix A**.

Superposition: The new algorithm relies upon the principle of superposition. Due to the close proximity among the magnetoelastic strips, the stress response of each magnetoelastic strip was found to be dependent on the loading conditions of neighboring strips, in addition to its own loading condition. Therefore, assuming the strip-to-strip cross interference is cumulative a series of equations were developed to relate applied force on a strip to measured 2nd order harmonic amplitude at each coil. A detailed description of these equations and the theory behind them can be found in section 2.4 of the appended journal article currently in review (see **Appendix A**).

Specific Aim 3: System Performance Evaluation

According to our initial plan, Specific Aim 3 will be conducted in full after completion of Specific Aim 1 and 2. Specifically, we will employ the sensor fabricated in Aim 1 into the detection system developed in Aim 2. The performance of the whole technology will then be evaluated and optimized.

Even though Aim 3 is not yet addressed completely, certain portions of the system have been reevaluated, out of necessity, and found to be insufficient for the continuation of the project. Specifically, previously, the use of a four shaft manual mechanical loader was reported. This loader proved to be insufficient for continuing work and a new mechanical loader and detection system have been developed. The new system consists of a fully automated four piston pneumatic mechanical loader and an additional automated three coil detection system, with the appropriate circuit elements and computer control programs.

Automated Mechanical Loader: **Fig. 5** illustrates the new mechanical loader. The outer frame of the loader was comprised of four stainless steel rods screwed into a delrin base and an aluminum top. The stainless steel rods provided necessary structural support and the aluminum top allowed for metal threading for screwing in the pneumatic pistons, which was necessary since screwing metal into plastic or plastic into metal is never ideal especially when the plastic/metal will be under loading. The rest of the system consisted of delrin in order to prevent the construction of a metallic frame which could create a shielding effect.

Force is applied by four delrin rods, with associated load cells, attached to stainless steel cylinders, screwed onto the piston shafts by slotted connector pieces custom built using a V-Flash FTI 230 Desktop Printer (3D Systems Corporation 333 3D Systems Circle, Rock Hill SC 29730). Pressure build up in the pistons causes the shafts and attached cylinders to extend. As

the cylinders move down, the hanging rods and load cells also move until contacting the sensor. As a result of the slot in the connector pieces, th e cylinders continue to move until reaching the load cells, thus applying force. This not only c reates a true zero loading condition , since the delrin rods hang from t he cylinders and do not initially con tact the sen sor, but also allows the application of different force profiles in four regions. In addit ion, a stepper motor, not pictured in **Fig. 5**, is attached to the plate on which the sensor sits, allowing for computer controlled rotation of sensors when testing from the front/back with a single set of detection coils.

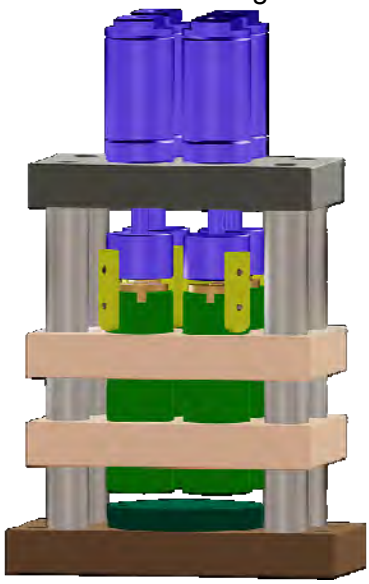

Fig. 5. The mechanical loader houses the sensor and is capable of providing different loading profiles in four regions.

Air flow to the pistons is controlled by a series of Clippard EVP series proportional control valves (Clippard Instrument Laboratory, Inc. 7390 Colerain Ave., Cinc innati, Ohio 45239). These solenoid type valves control air flow as a fun ction of applied voltage, with zero volts completely closing the valve and ten volts completely opening the valves. Air coming from the main source enters into the control box where it is split between two T junctions, essentially creating four lines of airflow. Each of the four air pathways i s then split again upon meeting the first of two EVP valves. The first valve acts as a main control for overall air volume control and splits the air between a piston and another EVP valve. The second valve acts as the primary control unit for force application. By opening or closing the second EVP valve, the total volume of air to the piston cha nges. A higher volume of air flow to the piston will result i n greater air pressure and, thus, a higher load, and vice versa. In total, the air flow control system consisted of eight EVP valves connected to four pneumatic pistons.

Loader Control Circuitry: The hard ware design for the n ew mechanical loader included four parallel digital proportional plus integral (PI) control units realized through the integration of a microcontroller (MSP430fg4618), an array of transistors for EVP actuation (2SD882) and load cells (FC2311) for feedback on the current loading state. Additionally, offset, gain and filtering stages were also implemented for design optimization and calibration.

For acquisition of load data, four Measurement Specialties FC23 250 lbf Compression Load Cells placed in series with the applied load and actuating pneumat ic cylinders. Differential amplifier configurations (LF353) then converted the amplified millivolt-level signals to achieve an output range of 0 to 2. 5 V, which could be measured by the microcontroller's analog-to-digital converter. Due to repeatability issue s with the lo ad cell offset voltages, a small offset (approx. 40 mV) wa s added to the amplified load cell voltage to account for its maximum negative

voltage offset and thus assure that all microcontroller inputs were positive. In combination with the negative offset-nulling circuit, the microcontroller software automatically compensated for the new positive offset at power-up and, as desired, between tests. This feature significantly improved the reliability of the force data, especially when collected over long durations.

In order to implement the desired loading control algorithm, a MSP430fg4618 microcontroller unit (MCU) was utilized. This microcontroller was selected due to its 250 ksps 12-bit analog-to-digital converter (ADC), low power operation, 16 MHz clock frequency and integrated SPI and UART peripherals. Additionally, previous knowledge regarding this microcontroller family played a key role in its selection. Although the MCU handles the control algorithm, a lack of digital-to-analog converter (DAC) channels on commercially available microcontrollers called for implementation of an external DAC7568 8-channel converter. The DAC chip was controlled by the MCU via a customized SPI interface in order to set the DC voltage level for each of eight EVP valves. Since the outputs of the DAC were from 0 to 3.3 V, supplementary circuitry was required to generate the 10 V signal necessary to fully open the EVP valves. For this purpose, voltage gain was achieved through LF353 operational amplifiers which were chosen for their low cost, low drift and high reliability and 2SD882 transistors were employed to provide the 200 mA current necessary to drive the EVP valves. With the combination of the MCU, DAC and amplification circuitry, full control of the EVP valves was possible.

Switching and Rotating Circuit: Currently, the overall system utilized a Spectrum/Network Analyzer, AC and DC supplies and high-power audio amplifiers in conjunction with an additional circuit which switched between three detection coils. The switching circuit was comprised of an MSP430f2618 which controls an 8-channel multiplexer. Simple digital switching between Spectrum Analyzer inputs was made possible by interfacing the microcontroller and multiplexer, with room for additional sensing coils in the future. While multiplexing the input signals was proven useful, the limitation of sampling only one coil at a time was a significant drawback on detection speed. Additionally, the use of external AC and DC power supplies significantly increased code complexity and system size.

Rotation of the detection platform was necessary to minimize the number of detection coils. Because the response of all strips from both the front and back were desired, a Portescap 55M048D2U stepper motor was implemented to rotate the platform between tests. The stepper motor was controlled by the MCU through a circuit generated by SparkFun electronics (EasyDriver Stepper Motor Driver). To avoid magnetic interference, the power to the motor was disabled digitally by the EasyDriver before measuring the sensor response.

Microcontroller Program: To maintain versatility in design, the MSP430 code was limited to a proportional plus integral controller that could receive commands from a master central processing unit (CPU), via standard RS-232 communication implemented on the MSP430's UART peripheral, as well as return load results. The microcontroller slave functions included receiving new load data, using the newest received load values, calibrating the load cell offsets and sending the current load state back to the CPU.

The proportional plus integral (PI) control function was carried out by modifying the DAC7568 output voltages via an SPI interface and detecting obtained load feedback by measuring the load cells connected to onboard ADC pins. A custom SPI protocol was written to provide necessary setup and transition times as the MSP430 peripheral interface was incapable of producing long enough transitions for DAC7568 interfacing. The control mechanism provided force by varying the voltage level of the EVP valve that allowed air to exit the cylinder. Increasing the voltage released more air from the cylinder resulting in a decreased load. By setting an initial voltage level at maximum outflow (no applied force) and adding the difference

between the current and the desired loads multiplied by some factor (the integration constant), an integral controller was developed.

Due to limitations of the maximum force output, the inflow air level, also controlled by EVP valves, was changed in proportion to the desired load magnitude. To accomplish this task, calibration curves were generated which yielded the fastest settling times and minimal current demands at a desired load level. By combining proportional control of the inflowing air rate with integral control of the outflow rate, a PI controller was generated which had the capacity to apply and measure loads ranging from 0 to 85 lbf on each of four loading regions.

In addition to calibrating the inflow air rate to the desired load, consideration of the total inflow rate for all loading regions was necessary. Because the air supply was regulated for 90 psi rather than flow rate, the flow rate varied according to the total need of all cylinders at a given instant. To compensate for this inconvenience, the inflow air rate was further regulated in software by increasing inflow rate with increasing total force application. This consideration allowed more stable settling times across varied loading parameters.

Computer Interface: Although the microcontroller was designed to achieve optimum settling times and stability across a range of loading profiles, a computer interface was required to set and update each load as well as recalibrate and receive the current load cell data. To perform this task, a Visual Basic 6.0 (VB6) interface was created to communicate to the control circuitry. The VB6 code allowed for entire loading profiles to be actuated and recorded to a file by simply entering the settling time, starting load on each cell, ending load on each cell and total number of steps to collect. Additionally, the code controlled the Spectrum Analyzer, AC and DC power supplies, in order to perform a DC biasing sweep of the loaded sensor response, and stored the data to a file.

Key Research Accomplishments

- Characterization 3 strip sensor grid
- Development of superposition based algorithm
- Preliminary testing of etched sensors
- Preliminary testing of trapezoidal and embedded sensors
- Construction and testing of new fully automated pneumatic loader systems
- Fully automated simultaneous data collection from multiple coils

Reported Outcomes

- Paper in submission (**Appendix A**)
- Based on the knowledge acquired through this work, we applied for, but did not receive, student fellowships from:
    - Michigan Space Grant Consortium
- Based on the knowledge acquired through this work, we applied for, and received, student fellowships from:
    - National Defense Science and Engineering Grant

Conclusion

To date, continuing research has demonstrated the efficacy of the sensor platform for use on hard surfaces with preliminary testing in embedded structures. At this phase, the project is heading towards testing which must be preceded by experiments with non-uniform Metglas strips and followed by more thorough testing with embedded sensors. An automated four cylinder mechanical loader apparatus was recently finished, with a single force applicator version already in use for characterizing a three strip sensor, and automated data collection from multiple coils has also been implemented in testing. Additionally, preliminary testing of trapezoidal and embedded sensors was also accomplished. Moreover, the excitation and detection circuits are now ready for integration and further developments in the use of electroplating and/or other processes to replace shearing/etching sensing elements continues.

These advances are important due to the lack of wireless long term monitoring systems available to medical staff, not just for lower limb prosthetics but also for other applications as well. While the application for this sensor system is a lower limb prosthesis, the technology can easily be adapted to monitor other devices, such as total knee arthroplasty implants. Moreover, the system is expected to be low cost and easy to implement and produce. Overall, this device could drastically improve the quality of care for lower limb amputees and assist in the further development of better prosthesis in addition to contributing to the understanding of the dynamic biomechanical loads associated with the stump-socket interface.

References

None

Appendix A: Submitted Paper for Review

A Wireless, Magnetoelastic-based Sensor Array for Force Monitoring on a Hard Surface

Brandon D. Pereles, Andrew J. DeRouin, Thomas A. Dienhart, Ee Lim Tan, Keat Ghee Ong*
Department of Biomedical Engineering, Michigan Technological University, Houghton, MI 49931, USA.
* Corresponding author: kgong@mtu.edu

Abstract – A force monitoring system consisting of stress-sensitive magnetoelastic strips for remotely measuring the force profile across a hard surface is described. Under the excitation of a magnetic AC field, the magnetoelastic strips generated higher-order harmonic fields (magnetic AC fields at multiple frequencies of the excitation field), allowing remote measurement of their responses without interference from the excitation field. Due to their magnetoelastic properties, these higher-order harmonic fields were also dependent on the applied force and, as a result, variations in force/stress could be tracked via changes in the field amplitudes. These changes were monitored using a detection system featuring a set of magnetic detection coils, which captured the response of the magnetoelastic strips. To demonstrate the functionality of this sensor system, a three-strip magnetoelastic sensor array was fabricated on a flat polycarbonate substrate. The substrate, placed within a customized mechanical loader, was exposed to a variety of force loading conditions. Experimental results demonstrated a proportional relationship between the amplitude of the 2nd order harmonic field and the applied force. An algorithm was developed to identify the magnitude of the applied force. The novelty of this system lies in its wireless and passive nature, which is ideal for applications in which wires and internal power sources are prohibited or discouraged. Moreover, the sensing component of this system is an array of thin magnetoelastic strips, allowing for minimal modifications to existing structures during implementation.

Keywords: Magnetic higher-order harmonic fields, magnetoelastic, wireless, passive, force sensors, mechanical loading.

1. Introduction

Force and stress are generally measured via strain, which is defined as the change in dimensions of an object due to an applied force. In practice, strain is often measured with strain gauges, most of which can be classified as resistive, capacitive, or vibrational. Resistive strain gauges monitor strain as a function of the change in resistance across a conductive or semiconductive material when elastically deformed [1]. Semiconductive materials exhibit piezoresistive behavior, resulting in a larger change in the electrical response with applied force compared to conductive materials [2]. As a result, semiconductive materials exhibit higher gauge factors, typically between 50 and 200, while conductive materials experience less than 5 [1]. These piezoresistive strain gauges find common use in different fields for a variety of applications, such as measuring stress on a knee prosthesis [3] or stress monitoring during an electronic packaging process [4]. While semiconductor strain gauges offer accurate sensing on small scales, their response can vary with temperature, and they can be difficult to manufacture.

Capacitive strain gauges measure stress/strain as a function of the change in the capacitance of a sensor. The primary advantages of capacitive strain gauges come from their capacity to operate in high temperature environments, minimal hysteresis, and long-term stability [4]. However, they have a lower sensitivity compared to their piezoresistive counterparts. For

example, thick cermet and polymer based capacitive strain gauges demonstrated similar linear responses and hysteresis to piezoresistive sensors but with gauge factors of only 6 for the cermet capacitor and 3.5 for the polymer capacitor [5].

Vibrating wire strain gauges function by measuring the vibrating frequency of a wire held in tension between two anchoring points and excited into vibration by a magnetic coil. Due to the effects of applied stress/strain, the anchoring position changes, resulting in a measurable alteration in vibrational frequency. [1]. Due to their high sensitivity, vibrating strain gauges are commonly used in low strain structures such as concrete beams [6]. As a whole, strain gauges in this category have the advantage of stress detection in the range of parts per million and are robust, easily attachable, and accurate; however, changes in temperature can drastically affect their performance [7].

Fiber optic technology has also been used for stress monitoring. The advantages of fiber optics include electrically passive operation, EMI immunity, high sensitivity, and multiplexing capabilities. Two main types of fiber optic strain sensors exist: interferometric and intensiometric. Interferometric methods observe changes in light passing through the fiber optic cable, while intensiometric sensing techniques monitor changes in the radiant power transmitted in a cable. A common example of an interferometric sensor is the Fabry-Perot interferometer sensor, which measures the change in light intensity between two mirrors placed in parallel with the fiber optic cable. An applied stress alters the distance between the mirrors resulting in a phase change in the light. While highly accurate, this method exhibits an inability to handle periodic interruptions by the power supply [8,9]. Additionally, fiber optic sensors are prone to damage, are affected by temperature elevations, and require that any coating used to protect fiber optic wires allow for proper transfer of force to the sensors [10].

Wireless capacitive stress/strain sensors were also developed for monitoring pressure as a function of change in measured capacitance. One such device coupled an RF transceiver to a custom capacitor for pressure monitoring [11]. The device was comprised of a pressure sensitive cavity, fabricated through silicon fusion bonding of two silicon wafers used to seal the cavity, and a flexible and a stationary electrode, forming a capacitor. Pressure applied to the device deflected the flexible electrode toward the fixed electrode, thus altering the capacitance of the sensor. Using a RF transceiver, information was wirelessly collected and sent for analysis [11]. Another wireless capacitive sensor, known as the SmartPill, incorporated pressure, pH, and temperature sensors for monitoring gastrointestinal tract conditions [12]. Unfortunately, these systems are limited in their size by the necessity for onboard electronics and, in the case of an active sensor, may eventually require the device to be removed in order to replace the power supply.

A simpler version of wireless capacitive stress/strain sensors was realized by incorporating an inductive-capacitive (LC) tank circuit into a sensor. In a wireless, passive stress/strain LC sensor, the capacitive stress/strain element connected to an inductor, which remotely conveyed stress/strain information as a change in the resonant frequency of the tank circuit. Among the applications of this type of sensor are monitoring stent integrity after an endovascular repair procedure [13] and measuring pressure in automobile tires [14].

Another class of passive stress/strain sensors is based on amorphous magnetoelastic materials. When exposed to a time varying AC field, magnetoelastic materials vibrate due to the magnetoelastic effect. The magnetoelastic effect also causes the vibrating magnetoelastic material to generate a magnetic flux that reaches a peak at its mechanical resonant frequency [15,16]. When an internal stress is applied, the resonant frequency of the strip becomes stress

dependent, and, as an example, has been used to determine atmospheric pressure [15,16]. This sensor is not only passive and wireless, but also low cost and long lasting. However, the strip itself must be stressed (by bending) to act as a sensor and there is no reliable way to control its sensitivity.

A strain sensor was developed using magnetoelastic materials by Kouzoudis and Mouzakis [17]. A Metglas 2826MB ribbon was attached on an epoxy resin slab and exposed to vibrations of varying amplitudes and frequencies. Due to its magnetoelastic property, the vibration of the magnetoelastic material caused a change in its magnetization stages, which was remotely picked up by a nearby detection coil. The sensor was demonstrated to have a strain gauge factor of 11,700 at a vibration frequency of 150 Hz.

Due to magnetic softness, amorphous magnetoelastic materials also generate higher order harmonic fields (magnetic fields at multiple frequencies of the excitation field) when under the excitation of a low frequency AC magnetic field [18]. To visualize the higher-order harmonic fields, the magnetoelastic material is generally excited by a steady AC magnetic field along with a sweeping DC biasing field. The biasing field alters the magnitude of the higher order harmonic fields and thus produces a distinct pattern as shown in **Figure 1**. In the previous work, it was shown that the amplitude of the higher-order harmonic fields increased when force was applied along the length of a magnetoelastic strip [19].

This paper describes a force monitoring system that tracked the changes in the 2nd order harmonic amplitudes of an array of magnetoelastic strips. By using an array of magnetoelastic strips, the new system is able to monitor not only the total contact force on the surface, but can also determine the force distribution on the surface. In contrast to the previous work [18], force was applied directly onto the surface instead of along the length of the magnetoelastic strip. Similar to the previous work, however, the application of force on the magnetoelastic strip surface resulted in an increase in the 2nd order harmonic field (see **Figure 1**).

By capturing the response of each strip, the system could identify the position and magnitude of the applied force. This sensing system was not only wireless and passive, but also simple to implement since it was nothing more than an array of magnetoelastic strips directly applied onto the desired surface. The process reduces cost and will allow for the production of long lasting sensors for a variety of applications.

It is worth noting that the presented sensor differs from other devices based on magnetoelastic materials, such as those described by Kouzoudis and Mouzakis [17], in terms of operating principle, ideal application, and strengths and weaknesses. For instance, to obtain good sensitivity, Kouzoudis' sensor system required the substrate to vibrate and the sensor sensitivity was also proportional to the vibrational frequency. The described sensor, on the other hand, does not require the substrate to vibrate, and its sensitivity is largely related to the magnetoelasticity of the material. Moreover, unlike Kouzoudis' system, the described sensor uses the higher-order harmonic signals from the material to track pressure and stress. The use of higher-order harmonic signals can significantly remove the background excitation signal, thus increasing the signal to noise ratio. Furthermore, the major applications for both technologies are different due to the differences in their operating principle. Thus, the described sensor is better suited for stress and pressure monitoring while Kouzoudis' sensor system is ideal for strain monitoring.

2. Experiments

2.1. Sensor Fabrication and Experimental Setup

The sensor, illustrated in **Figure 2**, was cut from a block of polycarbonate material and measured 47 mm × 56.5 mm × 12.2 mm. Metglas 2826MB ribbon ($Fe_{40}Ni_{38}Mo4B_{18}$), purchased from Metglas Inc, Conway, SC, USA, was used as the magnetoelastic stress sensing material due to its large magnetostriction (>12 ppm), high permeability (>50,000), and low magnetic coercivity. Three sensing strips were sheared from a 26 μm thick Metglas ribbon to 50 mm × 5 mm, and were adhered to the upper surface of the block using cellulose adhesive tape (50 μm thick). Adhesive tape was found to introduce less internal stress than glue or epoxy, thus preserving sensor-to-sensor reproducibility. For convenience, these sensing strips were labeled Strip 1, 2, and 3 respectively.

An automated pneumatic mechanical loader (see **Figure 3**) was constructed to apply controllable force to each strip of the sensor. **Figure 3** also illustrates the control elements of the automated system. A manual air control valve allowed for adjustments to the overall air flow into the apparatus. Following the main valve, the air was split between an EVP series Proportional Control Valve (Clippard Instrument Laboratory, Inc. 7390 Colerain Ave., Cincinnati, Ohio 45239) and a pneumatic piston. Opening or closing the EVP valve by increasing or decreasing the voltage from a connected Kepco 10V Programmable Power Supply altered the volume of air flowing to the pneumatic piston. This in turn affected the force applied by the piston. Applied force was monitored using a Measurement Specialties FC23 Compression Load Cell, placed between the load applicator plate and the piston. An Extech 382202 DC Power Supply provided the input voltage to the load cell and applied force data was monitored and transferred to a PC using a Hewlett Packard 3478A Multimeter. A custom Visual Basic program calculated the difference between the actual applied force and the desired force which was then altered using an integral control algorithm to produce an appropriate change in voltage to be sent to the EVP valve. The system provided repeatable loading with a range of 0-355.86 N and was capable of adjusting the force by 4.44 N ± 1.11 N. In addition to automated force loading, the system and Visual Basic program allowed for simultaneous collection of sensor responses from the detection coils. It is worth noting that the range and weight increment of the system were set for the purposes of this testing by adjusting the air pressure into the system, the air flow at the main regulator, the coefficient used in calculating the change in voltage to the EVP valve, and the time allowed between weight increments for the system to settle.

Rectangular detection coils consisted of a functioning coil connected to an oppositely wound compensating coil in series, both made of 100 turns of 36 gage copper wire. The individual coils measured 12.0 mm × 17.6 mm × 4.3 mm. For convenience, the detection coils were labeled Coil 1, 2, and 3 according to the strip being measured (see **Figure 2**), and the compensating coils were similarly labeled Compensating Coil 1, 2, and 3. During the experiments, Strip 1, 2, and 3 were aligned to the centers of Coil 1, 2, and 3, respectively.

The sensor was secured within the mechanical loader and the apparatus was positioned directly in front of the detection and excitation coils. As illustrated in **Figure 4**, the detection coils were connected to an Agilent spectrum /network analyzer 4396B to capture the signal for the PC (through a custom Visual Basic program and GPIB interface) for further analysis. The excitation coils consisted of two superimposed 50 turn 18-gauge coils (28 cm in diameter) that provided the AC and DC excitation fields. One coil was connected to an AC function generator (Fluke 271 10 MHz) and an amplifier (Tapco J1400), while the other coil (DC) connected to a Kepco MBT 36-10 MT power supply. In all tests the AC field was 150 A/m, 200 Hz and the DC field was 0 - 250 A/m.

2.2. Experimental Procedure

The response of each magnetoelastic strip was collected while the total applied load increased from 0 to 266.89 N and then decreased to 0 N at weight increments of 22.24 N. During the experiment, data was collected simultaneously from all coils following a short period to allow the piston to reach the desired load and stabilize there. The collected data was then zeroed to a common starting point by subtracting a zero load value obtained from the first data point. This procedure was repeated for a variety of loading conditions created by placing rubber inserts over specified strips, thus producing conditions where in some strips were loaded and others were not.

In addition to changing with the application of force, the response of the sensing strips also varied as a function of relative location from the detection coils. To investigate the effect of changing sensor location, strip responses were measured while moving the mechanical loader incrementally on the x, y, and z axes of a rectangular coordinate system. The origin of the coordinate system was defined as the exact center between Coil 2 and Compensating Coil 2 (see **Figure 3** and **Figure 4**).

2.3. Stress Sensing Theory

The pressure sensitivity of the magnetically soft magnetoelastic material can be explained by the magnetic susceptibility (χ), which is the ratio of saturation magnetization (M_s) to anisotropy field (H_k) expressed as [20]:

$$\chi = M_s / H_k \tag{1}$$

The anisotropy field of a magnetic material can be related to the tensile stress along the magnetization direction as [16]:

$$H_k = H_{k0} - 3\lambda_s \sigma_y / M_s \tag{2}$$

where H_{k0} is the anisotropy field at zero stress, λ_s is the saturation magnetostriction of the material, and σ_y is the tensile stress along the magnetization direction, which is also along the length of the sensor.

Eq. (2) describes the change in anisotropy field due to the tensile stress along the sensor's length; however, for this particular application, force was loaded on the dominant surface of the ribbon shape sensor (along the z-direction shown in **Figure 2**). Therefore, the transverse stress on the sensor surface (z-direction) was related to the tensile stress along the sensor length (y-direction) using the Poisson's ratio υ as:

$$\sigma_z = 2\sigma_y / \upsilon \tag{3}$$

Note that a scaling factor of two was added in Eq. (3) to compensate for the fact that only one side of the sensor was being stressed.

As shown in Eq. (2), increasing stress decreases the anisotropy field of a magnetic material, assuming the anisotropy energy and the saturation magnetization stay constant. The change in anisotropic field has a direct impact on the measured signal amplitude of the n-th order magnetic harmonic field (A_n), in Volts, which can be described by the equation [17]:

$$A_n = \frac{LB_s\omega}{\pi^2}\left| e^{jn\pi H_{dc}/h_{ac}} \cos(n\pi) - \frac{h_{ac}}{n\pi H_k}\sin\left(\frac{n\pi H_k}{h_{ac}}\right)\right| \tag{4}$$

where L is a variable that accounts for sensor-coil coupling, B_s is the saturation induction flux (for ferromagnetic materials, $B_s \approx M_s$), ω is the radian frequency of the fundamental order, h_{ac} is

the AC excitation field, and H_{dc} is the DC biasing field. Under an externally applied load, the sensor material deforms and generates an internal stress. Eqs. (1) – (4) indicate that stress causes a change in magnetic anisotropy, which alters magnetization and changes the higher-order magnetic fields allowing for remote detection of pressure.

As indicated in Eqs. (1) and (2), χ is inversely proportional to H_k, which decreases linearly with increasing σ_z. As a result, the susceptibility of the material is expected to show an exponential pattern with increasing stress and eventually converge on an asymptote at infinity as H_k approaches zero. While theoretically this represents an infinite increase in susceptibility, and thus an infinite increase in the 2nd order harmonic amplitude, realistically the change in the susceptibility and the 2nd order harmonic amplitude will more likely resemble an upper bounded decaying exponential curve since the susceptibility will experience a much slower change when the anisotropy has reached a near zero state.

2.4. Determination of the Force Loading

An algorithm was developed to determine the force loading on each magnetoelastic strip based on the measured 2nd order harmonic amplitudes. Since the measured 2nd order harmonic amplitudes of the magnetoelastic strips were expected to follow an upper bounded decaying exponential function with increasing stress, upper bounded decaying exponential curves were used to fit the measured data. Due to the close proximity of the magnetoelastic strips to one another, the stress response of each magnetoelastic strip was also dependent on the loading conditions of its neighboring strips. This result is expected, based upon the simple fact that neighboring magnetic fields will interact with one another. Therefore, assuming the strip-to-strip cross interference is cumulative at a given detection coil, the measured 2nd order harmonic amplitude of magnetoelastic Strip i (measured by the i^{th} detection coil) was represented by the summation of the responses of all strips as:

$$S_i = \sum_{j=1}^{3} A_{ij}\left(1 - e^{-a_{ij} f_j}\right) \tag{5}$$

where S_i is the measured 2nd order harmonic amplitude at Coil i, A_{ij} is the peak amplitude measured at Coil i when only strip j is at the maximum loading, a_{ij} is the decay coefficient (at Coil i when strip j is loaded), and f_j is the applied force at Strip j.

Eq. (5) consists of three upper bounded decaying exponential equations with three unknowns. To solve Eq. (5), a simple iterative method was developed to identify f_j for a set of given S_i. Starting with a set of estimated force loading, the iterative process determines the difference (δ_i) between the calculated S_i from Eq. (5) and the measured signal S_i as:

$$\delta_i = S_i(Calculated) - S_i(Measured) = \sum_{j=1}^{3} A_{ij}\left(1 - e^{-a_{ij} f_j}\right) - S_i(Measured) \tag{6}$$

A zero δ for all strips indicates the correct input for the force loadings; in contrast, a non-zero δ indicates there is an error in the calculated force loadings. The erroneous force loading g_j is determined from δ_i as:

$$\delta_i = A_{ij}\left(1 - e^{-a_{ij} g_j}\right) \tag{7}$$

The new estimated force loading f_j^{t+1} is determined by subtracting the current force loading to the erroneous force loading g_j:

$$f_j^{t+1} = f_j - g_j = f_j + \frac{\log\left(1-\delta_i / A_{ij}\right)}{a_{ij}} \tag{8}$$

Eq. (6) and (7) are iteratively solved until $f_j^{t+1} - f_j < \varepsilon$, where ε is the acceptable error of the iterative solution.

3. Results and Discussion

Figure 5 plots the signal recorded by Coil 1, 2, and 3 when rubber inserts were placed on Strip 1 (**Figure 5a**), 2 (**Figure 5b**), or 3 (**Figure 5c**), respectively. These results indicate that when the magnetoelastic strips were under direct force loading, the signal recorded by their corresponding coils increased following an upper bounded decaying exponential function: $a(1-e^{-x})$, confirming the theoretical behavior of the strips described previously. Also noticeable is that in **Figure 5a**, the stress response measured at Coil 2 was not zero, but instead was about 25% of the stress response measured at Coil 1, even though Strip 2 was not loaded. This is due to interference from Strip 1. In contrast, Coil 3 measured a zero response because the interference from Strip 1 was shielded by Strip 2 before reaching Strip 3. **Figure 5c** shows a similar response as **Figure 5a** since the sensor was symmetrical; however, the response at Coil 3 was slightly lower compared to Coil 1 due to minor differences in physical dimensions between Coil 1 and 3.

Similarly, **Figure 5b** indicates that Strip 2 interfered with measurements at Coil 1 and 3. Ideally, the measurements at Coil 1 and 3 should be identical but the response at Coil 3 was slightly smaller than Coil 1 due to differences in coil dimensions. Also, compared to **Figure 5a**, the change in harmonic amplitude was higher when Strip 2 was loaded since Strip 2's response was interfered with by both Strip 1 and 3, while in **Figure 5a** only Strip 1 interfered significantly with Strip 2.

After determining the coefficients A_{ij} and a_{ij}, the performance of the iteration process was examined. To prevent measurement errors from affecting the iteration process, all input measurements S_i were calculated using Eq. (5). **Figure 6** plots the estimated force loadings for all strips at each iteration step (initial force loadings were set to zero). It was found that the performance of the iteration process degraded with increasing force loading and that in the worst case scenario (156.58 N loading), the error (ε) was 0.35% after 1000 iterations and 0.0075% after 2000 iterations.

To determine the performance of the whole sensor system, all magnetoelastic strips were loaded and the responses from Coil 1, 2, and 3 were measured simultaneously. The measurements were then fed into Eqs. (6) and (8) to iteratively solve for the force loading on each strip. **Figure 7** plots the absolute percentage error between the actual and calculated forces on all strips at different force loading conditions. Although the iteration process has an error of only 0.0075% after 2000 iterations, due to uncertainties in the measured data and other experimental errors, the calculated force has a 10% error when compared to the measured force. One source of error was from the current method of force application. Rubber inserts were used to distribute load on the strips. When the rubber inserts were placed on different strips, the force distribution was assumed to be equally distributed among the strips. In practice, some strips may experience more force than the others due to slight imbalances of the loading plate. As a result, the measured force on each strip might vary slightly from the actual load on the strip. Another source of error was the exponential nature of the data. As shown in **Figure 5**, the sensitivity of the sensor decreased with increasing force loading as the upper bounded decaying exponential

curve saturated. As a result, the accuracy of the sensor decreased, especially in high load regions, leading to larger errors.

In addition to characterizing the sensor response under loading and analyzing the developed algorithm, the effects of movement on sensor response were also analyzed. The signal at Coil 2 was recorded and presented in **Figure 8** when the sensor was incrementally moved on the *x*, *y*, and *z* axes. While moving along the *x* axis, the measured amplitude increased when each sensing strip was closer to the center of the coil and then decreased as that center passed. This result was observed three times (corresponding to the 3 strips) followed by a sharp decrease toward zero. A similar result was seen along the *z* axis; however, in this case the rising and falling of the response occurred as Strip 2 moved within Coil 2 and Compensating Coil 2. As expected, the *y* axis testing demonstrated a gradual signal decrease with distance.

From **Figure 8**, it is evident that the location of the detection coils played a critical role in the accuracy of the system. In the experiment, the location of the sensor was fixed with respect to the detection/excitation coils. However, in practical use, the user may not be able to position the detection coils accurately. To ensure integrity of the measurement, the user will be able to move the coils around the sensor until the system picks up the maximum signal, indicating the correct orientation of the sensor. Alternatively, it is possible to place a calibration sensing strip, which can be parallel to the stress-responsive sensing strips but at a position that is insulated from force loading, such that all measurement data is calibrated from the calibration sensing strip to eliminate the location effect.

4. Conclusion

The fabrication and testing of a wireless passive sensor system for monitoring the applied force on a hard surface has been presented. The sensor was tested from 0 to 226.89 N with experimental data demonstrating an exponential increase in the 2nd order harmonic amplitude of magnetoelastic sensing strips as pressure increased. It was demonstrated that neighboring strips have an interference effect which contributes to the overall sensor reading at a given coil. Additionally, a simple iterative algorithm was developed to determine the applied force on all sensing strips by examining the signals captured by the detection coils.

Future works include the design and fabrication of a more complicated sensor, which will include strips forming a sensing grid, and a more sophisticated algorithm to accommodate the more complex sensor structure. In addition, a new process, such as electroplating or screen printing, will be developed for fabrication of the sensing strips to reduce sensor-to-sensor variability.

Acknowledgements

The authors would like to acknowledge the financial support from the Department of Defense (DOD) of the Office of the Congressionally Directed Medical Research Programs (CDMRP), Grant DR081026 Hypothesis Development.

References

1. A. L. Window, *Strain gauge technology*, Springer, New York **(1992)**.
2. R. L. Hannah and S. E. Reed, *Strain Gauge User's Handbook*, Springer, New York **(1994)**.
3. M. C. Hsieh, Y. K. Fang, M. Ju, G. Chen, J. Ho, C. H. Ya ng, P. M. Wu, G. S. Wu, T. Y. Chen, Journal of Microelectromechanical Systems 10(1) 121-127 **(2001)**.
4. K. Tian, Z. W ang, M. Zhang, L. Liu, IEEE Trans. on Co mponents and Packaging Technologies 32(2) 513-520 **(2008)**.
5. K. I. Arshak, D. McDonagh and M. A. Durcan Sensors and Actuators 79 102-114 **(2000)**.
6. S. A. Neild, M. S. Williams and P. D. McFadden, Strain 41(1) 3-9 **(2005)**.
7. D. Kuhunek and I. Zoric, IEEE Instrum entation and Measurem ent Technology Conference Proc. 1-4 **(2007)**.
8. Q. Shi, Z. Wang, L. Jin, Y. Li, H. Zha ng, F. Lu, G. Kai, X. Dong, IEEE Photonics Technology Letters 20(15) 1329-1331 **(2008)**.
9. Y. Huang, J. Tsai and F. Lee, ICM2007 4th IEEE Int. Conf. on Mechatronics 1-6 **(2007)**.
10. A. D. Kersey, M. A. Davis, H. J. Patrick, M. LeBlanc, K. P. Koo, C. G. Askins, M. A. Putnam and E. J. Friebele, Journal of Lightwave Technology 15(8) 1442-1463 **(1997)**.
11. K. Arshak, E. Jafer, T. McGloughlin, T. Corb ett, S. Chatzandroulis and D. Goustouridis, IEEE Sensors 28-31 **(2007)**.
12. A. Arshak, K. Arshak, D. W aldron, D. Morr is, O. Korostynska, E. Jafer and G. Lyon, Medical Engineering & Physics 27 347–356 **(2005)**.
13. J. Zhai, T. V. How and B. Hon, CIRP Annals - Manufacturing Technology 59(1) 187-190 **(2010)**.
14. M. Nabipoor and B. Y. Majlis, Journal of Physics: Conference Series 34(1) 770 **(2006)**.
15. C. A. Grimes, C. S. Mungle, K. Z eng, M. K. Jain, W. R. Dreschel, M. Paulose and K. G. Ong, Sensors 2 294-313 **(2002)**.
16. D. Kouzoudis and C. A. Grimes, Smart Mater. Struct. 9 1-5 **(2000)**.
17. D. Kouzoudis, D. E. Mouzakis, Sens. Actuators A 127(2) 355-359 **(2006)**.
18. E. L. Tan, B. D. Pereles and K. G. Ong, IEEE Sensors Journal 10(6) 1085-1090 **(2010)**.
19. K. G. Ong and C. A. Grimes, Sensors and Actuators A 101 49-61 **(2002)**.
20. J. D. Livingston, Phys. Stat. Sol. 70(2) 591–596 **(1982)**.

Figure Captions

Figure 1. The (a) 2nd order harmonic field and (b) 3rd order harmonic field measured as a function of an applied DC field with and without an applied force.

Figure 2. The sensor was comprised of three magnetoelastic sensing strips affixed to a polycarbonate substrate.

Figure 3. The mechanical loader housed the sensor and allowed for incremental loading of the sensing strips. The total applied force was measured with a load cell.

Figure 4. The full experimental setup illustrating the excitation coils and the detection coils. During the experiments, the mechanical loader (not shown here) and the test substrates were placed directly in front of the detection coils so Strip 1, 2, and 3 were directly aligned to Coil 1, 2, and 3, respectively.

Figure 5. Changes in the 2nd order harmonic amplitude captured by Coil 1, 2, and 3 when only Strip 1 (a), 2 (b), or 3 (c) was loaded, respectively.

Figure 6. Force loading on the magnetoelastic strips estimated by the iterative process as a function of iteration step. The numbers in the figure are the expected forces.

Figure 7. The percentage error between the actual and calculated forces on all strips at different force loading conditions.

Figure 8. Response of sensor when incrementally moved along the *x*, *y*, and *z*-axes.

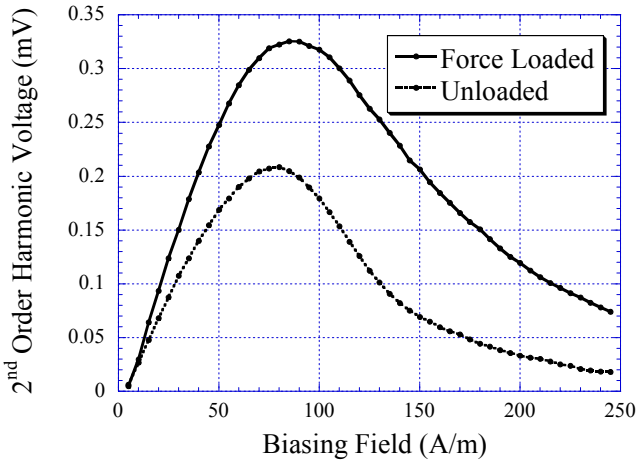

Figure 1a.

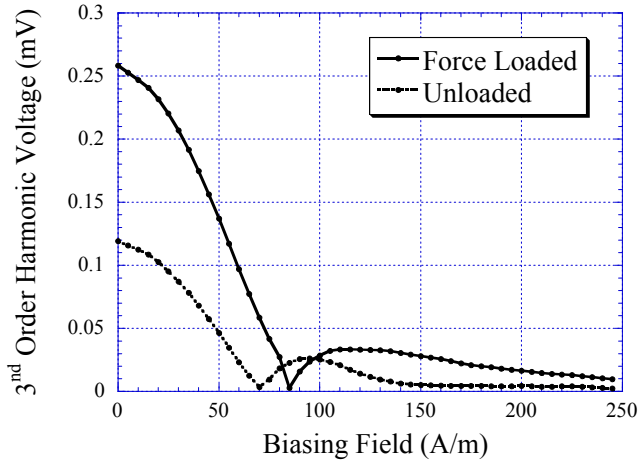

Figure 1b.

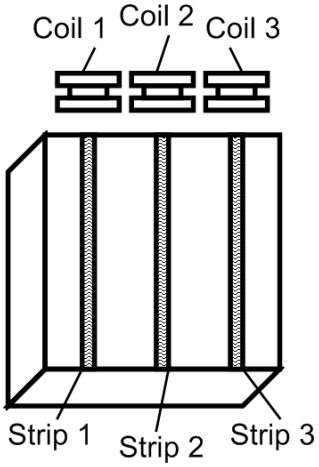

Figure 2.

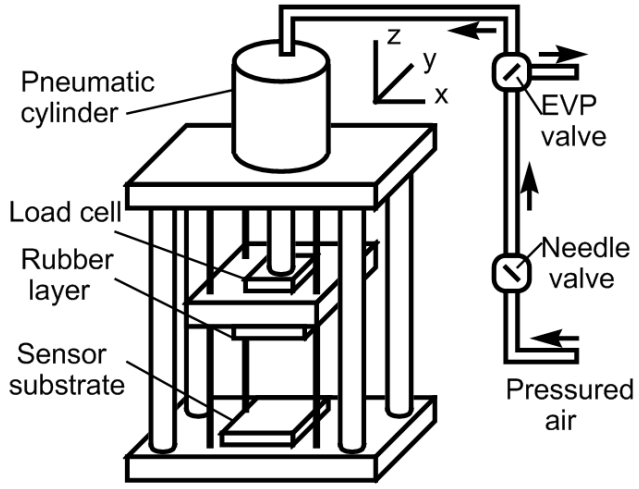

Figure 3.

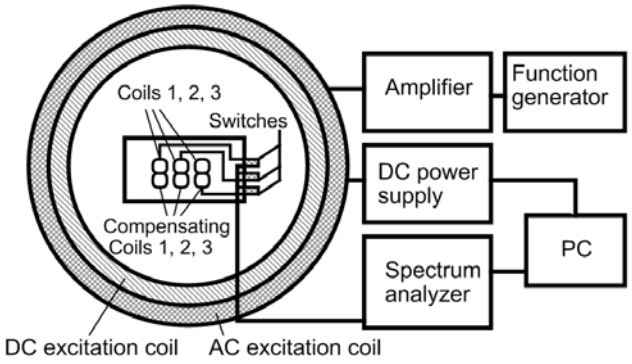

Figure 4.

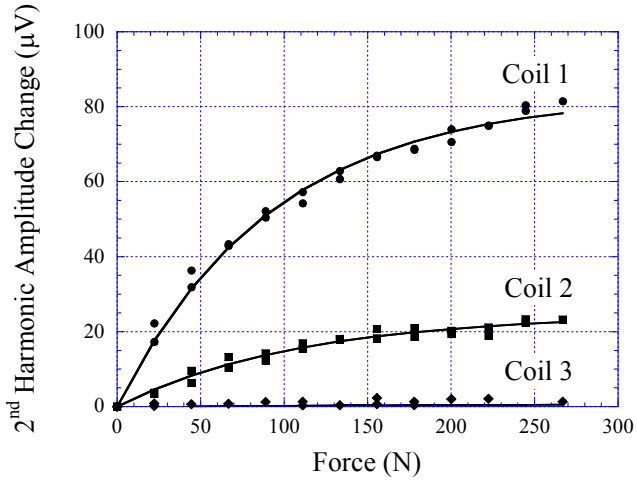

Figure 5a.

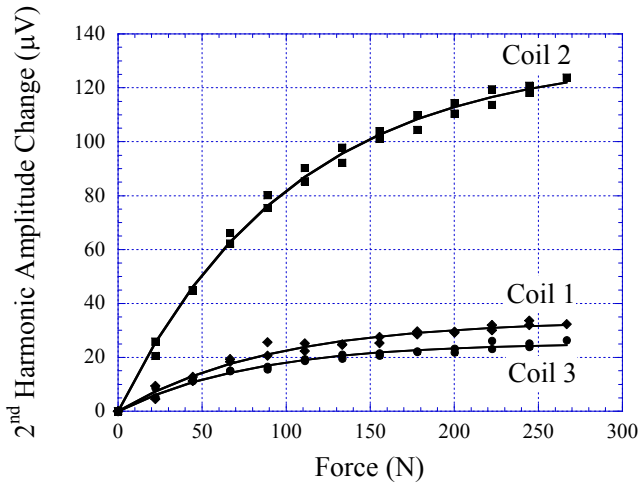

Figure 5b.

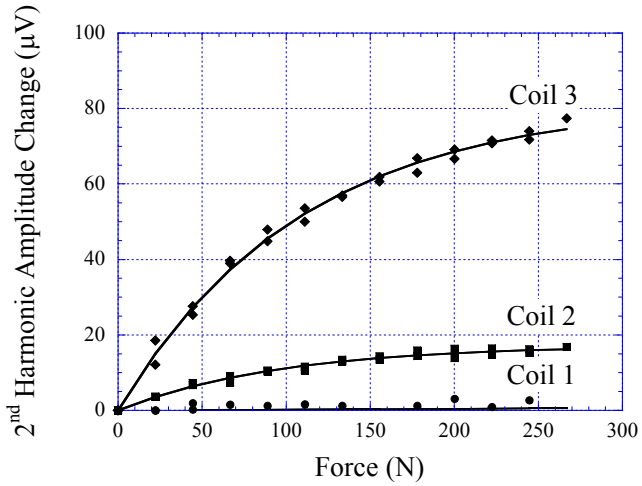

Figure 5c.

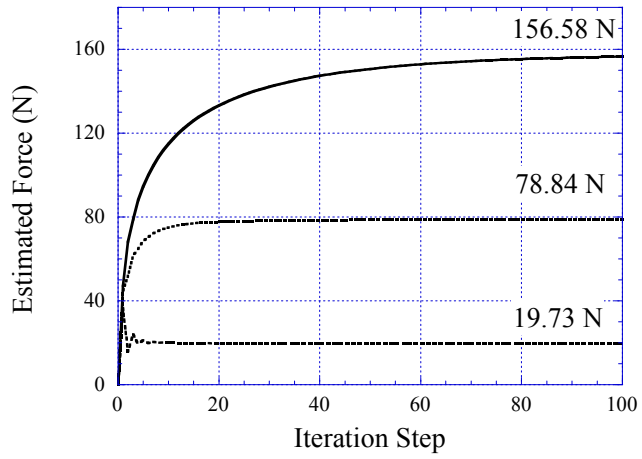

Figure 6.

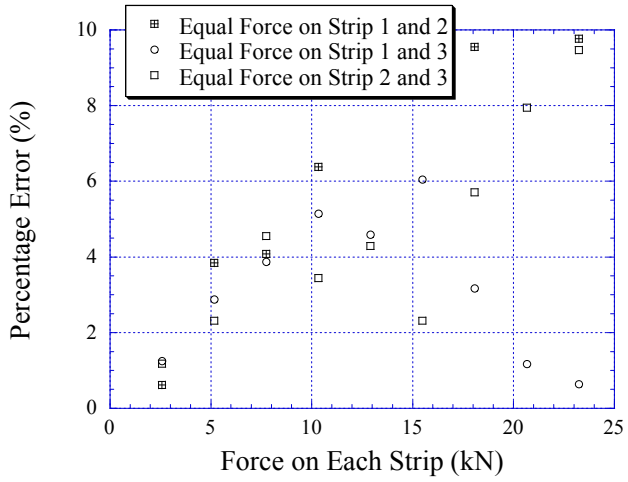

Figure 7.

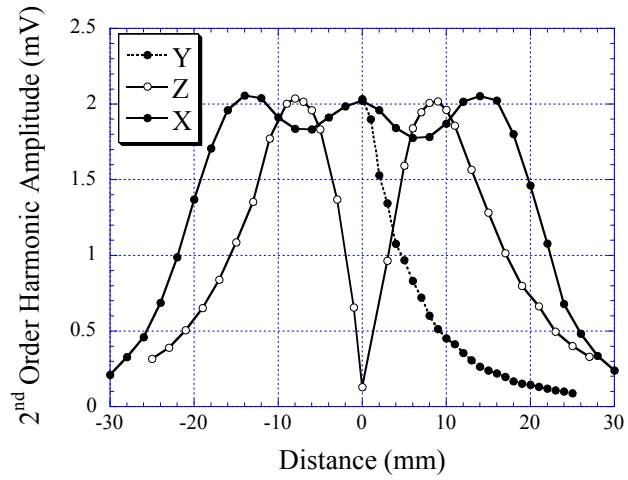

Figure 8.